References

Bader M, Peters J, Baltatu O, Muller DN, Luft FC, Ganten D (2001) Tissue renin-angiotensin systems: new insights from experimental animal models in hypertension research. J Mol Med 79:76–102

Baker KM, Booz GW, Dostal DE (1992) Cardiac actions of angiotensin II: role of an intracardiac renin-angiotensin system. Annu Rev Physiol 54:227–241

Bendig G, Grimmler M, Huttner IG, Wessels G, Dahme T, Just S, Trano N, Katus HA, Fishman MC, Rottbauer W (2006) Integrin-linked kinase, a novel component of the cardiac mechanical stretch sensor, controls contractility in the zebrafish heart. Genes Dev 20:2361–2372

Billet S, Bardin S, Verp S, Baudrie V, Michaud A, Conchon S, Muffat-Joly M, Escoubet B, Souil E, Hamard G, Bernstein KE, Gasc JM, Elghozi JL, Corvol P, Clauser E (2007) Gain-of-function mutant of angiotensin II receptor, type 1A, causes hypertension and cardiovascular fibrosis in mice. J Clin Invest 117:1914–1925

Bond RA, Ijzerman AP (2006) Recent developments in constitutive receptor activity and inverse agonism, and their potential for GPCR drug discovery. Trends Pharmacol Sci 27:92–96

Boucard AA, Roy M, Beaulieu ME, Lavigne P, Escher E, Guillemette G, Leduc R (2003) Constitutive activation of the angiotensin II type 1 receptor alters the spatial proximity of transmembrane 7 to the ligand-binding pocket. J Biol Chem 278:36628–36636

Brancaccio M, Fratta L, Notte A, Hirsch E, Poulet R, Guazzone S, De Acetis M, Vecchione C, Marino G, Altruda F, Silengo L, Tarone G, Lembo G (2003) Melusin, a muscle-specific integrin beta1-interacting protein, is required to prevent cardiac failure in response to chronic pressure overload. Nat Med 9:68–75

Cohn JN, Tognoni G (2001) A randomized trial of the angiotensin-receptor blocker valsartan in chronic heart failure. N Engl J Med 345:1667–1675

Costa T, Herz A (1989) Antagonists with negative intrinsic activity at delta opioid receptors coupled to GTP-binding proteins. Proc Natl Acad Sci USA 86:7321–7325

Feng YH, Miura S, Husain A, Karnik SS (1998) Mechanism of constitutive activation of the AT1 receptor: influence of the size of the agonist switch binding residue Asn(111). Biochemistry 37:15791–15798

Gether U (2000) Uncovering molecular mechanisms involved in activation of G protein-coupled receptors. Endocr Rev 21:90–113

Groblewski T, Maigret B, Larguier R, Lombard C, Bonnafous JC, Marie J (1997) Mutation of Asn111 in the third transmembrane domain of the AT1A angiotensin II receptor induces its constitutive activation. J Biol Chem 272:1822–1826

Harada K, Komuro I, Shiojima I, Hayashi D, Kudoh S, Mizuno T, Kijima K, Matsubara H, Sugaya T, Murakami K, Yazaki Y (1998a) Pressure overload induces cardiac hypertrophy in angiotensin II type 1A receptor knockout mice. Circulation 97:1952–1959

Harada K, Komuro I, Zou Y, Kudoh S, Kijima K, Matsubara H, Sugaya T, Murakami K, Yazaki Y (1998b) Acute pressure overload could induce hypertrophic responses in the heart of angiotensin II type 1a knockout mice. Circ Res 82:779–785

Karnik SS, Gogonea C, Patil S, Saad Y, Takezako T (2003) Activation of G-protein-coupled receptors: a common molecular mechanism. Trends Endocrinol Metab 14:431–437

Knoll R, Hoshijima M, Hoffman HM, Person V, Lorenzen-Schmidt I, Bang ML, Hayashi T, Shiga N, Yasukawa H, Schaper W, McKenna W, Yokoyama M, Schork NJ, Omens JH, McCulloch AD, Kimura A, Gregorio CC, Poller W, Schaper J, Schultheiss HP, Chien KR (2002) The cardiac mechanical stretch sensor machinery involves a Z disc complex that is defective in a subset of human dilated cardiomyopathy. Cell 111:943–955

Komuro I, Yazaki Y (1993) Control of cardiac gene expression by mechanical stress. Annu Rev Physiol 55:55–75

Kudoh S, Komuro I, Hiroi Y, Zou Y, Harada K, Sugaya T, Takekoshi N, Murakami K, Kadowaki T, Yazaki Y (1998) Mechanical stretch induces hypertrophic responses in cardiac myocytes of angiotensin II type 1a receptor knockout mice. J Biol Chem 273:24037–24043

Kung C (2005) A possible unifying principle for mechanosensation. Nature 436:647–654

Lee MA, Bohm M, Paul M, Ganten D (1993) Tissue renin-angiotensin systems. Their role in cardiovascular disease. Circulation 87: IV7–13

Levy D, Garrison RJ, Savage DD, Kannel WB, Castelli WP (1990) Prognostic implications of echocardiographically determined left ventricular mass in the Framingham Heart Study. N Engl J Med 322:1561–1566

Lindholm LH, Ibsen H, Dahlof B, Devereux RB, Beevers G, de Faire U, Fyhrquist F, Julius S, Kjeldsen SE, Kristiansson K, Lederballe-Pedersen O, Nieminen MS, Omvik P, Oparil S, Wedel H, Aurup P, Edelman J, Snapinn S (2002) Cardiovascular morbidity and mortality in patients with diabetes in the Losartan Intervention For Endpoint reduction in hypertension study (LIFE): a randomised trial against atenolol. Lancet 359:1004–1010

Martin SS, Holleran BJ, Escher E, Guillemette G, Leduc R (2007) Activation of the angiotensin II type 1 receptor leads to movement of the sixth transmembrane domain: analysis by the substituted cysteine accessibility method. Mol Pharmacol 72:182–190

Miura S, Karnik SS (2002) Constitutive activation of angiotensin II type 1 receptor alters the orientation of transmembrane helix-2. J Biol Chem 277:24299–24305

Miura S, Feng YH, Husain A, Karnik SS (1999) Role of aromaticity of agonist switches of angiotensin II in the activation of the AT1 receptor. J Biol Chem 274:7103–7110

Miura S, Saku K, Karnik SS (2003a) Molecular analysis of the structure and function of the angiotensin II type 1 receptor. Hypertens Res 26:937–943

Miura S, Zhang J, Boros J, Karnik SS (2003b) TM2-TM7 interaction in coupling movement of transmembrane helices to activation of the angiotensin II type-1 receptor. J Biol Chem 278:3720–3725

Miura S, Fujino M, Hanzawa H, Kiya Y, Imaizumi S, Matsuo Y, Tomita S, Uehara Y, Karnik SS, Yanagisawa H, Koike H, Komuro I, Saku K (2006) Molecular mechanism underlying inverse agonist of angiotensin II type 1 receptor. J Biol Chem 281:19288–19295

Orr AW, Helmke BP, Blackman BR, Schwartz MA (2006) Mechanisms of mechanotransduction. Dev Cell 10:11–20

Perez DM, Karnik SS (2005) Multiple signaling states of G-protein-coupled receptors. Pharmacol Rev 57:147–161

Pfeffer MA, Swedberg K, Granger CB, Held P, McMurray JJ, Michelson EL, Olofsson B, Ostergren J, Yusuf S, Pocock S (2003) Effects of candesartan on mortality and morbidity in patients with chronic heart failure: the CHARM-Overall programme. Lancet 362:759–766

Sadoshima J, Xu Y, Slayter HS, Izumo S (1993) Autocrine release of angiotensin II mediates stretch-induced hypertrophy of cardiac myocytes in vitro. Cell 75:977–984

Senbonmatsu T, Ichihara S, Price Jr E, Gaffney FA, Inagami T (2000) Evidence for angiotensin II type 2 receptor-mediated cardiac myocyte enlargement during in vivo pressure overload. J Clin Invest 106:R25–29

Tanimoto K, Sugiyama F, Goto Y, Ishida J, Takimoto E, Yagami K, Fukamizu A, Murakami K (1994) Angiotensinogen-deficient mice with hypotension. J Biol Chem 269:31334–31337

Timmermans PB, Wong PC, Chiu AT, Herblin WF, Benfield P, Carini DJ, Lee RJ, Wexler RR, Saye JA, Smith RD (1993) Angiotensin

II receptors and angiotensin II receptor antagonists. Pharmacol Rev 45:205–251

Vilardaga JP, Steinmeyer R, Harms GS, Lohse MJ (2005) Molecular basis of inverse agonism in a G protein-coupled receptor. Nat Chem Biol 1:25–28

White DE, Coutu P, Shi YF, Tardif JC, Nattel S, St Arnaud R, Dedhar S, Muller WJ (2006) Targeted ablation of ILK from the murine heart results in dilated cardiomyopathy and spontaneous heart failure. Genes Dev 20:2355–2360

Wu L, Iwai M, Nakagami H, Chen R, Suzuki J, Akishita M, de Gasparo M, Horiuchi M (2002) Effect of angiotensin II type 1 receptor blockade on cardiac remodeling in angiotensin II type 2 receptor null mice. Arterioscler Thromb Vasc Biol 22:49–54

Yamano Y, Ohyama K, Chaki S, Guo DF, Inagami T (1992) Identification of amino acid residues of rat angiotensin II receptor for ligand binding by site directed mutagenesis. Biochem Biophys Res Commun 187:1426–1431

Yamazaki T, Komuro I, Kudoh S, Zou Y, Shiojima I, Mizuno T, Takano H, Hiroi Y, Ueki K, Tobe K (1995) Angiotensin II partly mediates mechanical stress-induced cardiac hypertrophy. Circ Res 77:258–265

Yamazaki T, Komuro I, Kudoh S, Zou Y, Shiojima I, Hiroi Y, Mizuno T, Maemura K, Kurihara H, Aikawa R, Takano H, Yazaki Y (1996) Endothelin-1 is involved in mechanical stress-induced cardiomyocyte hypertrophy. J Biol Chem 271:3221–3228

Yao X, Parnot C, Deupi X, Ratnala VR, Swaminath G, Farrens D, Kobilka B (2006) Coupling ligand structure to specific conformational switches in the beta2-adrenoceptor. Nat Chem Biol 2:417–422

Zou Y, Komuro I, Yamazaki T, Kudoh S, Uozumi H, Kadowaki T, Yazaki Y (1999) Both Gs and Gi proteins are critically involved in isoproterenol-induced cardiomyocyte hypertrophy. J Biol Chem 274:9760–9770

Zou Y, Akazawa H, Qin Y, Sano M, Takano H, Minamino T, Makita N, Iwanaga K, Zhu W, Kudoh S, Toko H, Tamura K, Kihara M, Nagai T, Fukamizu A, Umemura S, Iiri T, Fujita T, Komuro I (2004) Mechanical stress activates angiotensin II type 1 receptor without the involvement of angiotensin II. Nat Cell Biol 6:499–506

Deficiency of *Myo18B* in mice results in embryonic lethality with cardiac myofibrillar aberrations

Rieko Ajima[1,a], Hiroshi Akazawa[2], Maho Kodama[3], Fumitaka Takeshita[3], Ayaka Otsuka[1], Takashi Kohno[1], Issei Komuro[2], Takahiro Ochiya[3] and Jun Yokota[1,*]

[1]*Biology Division and* [3]*Section for Studies on Metastasis, National Cancer Center Research Institute, Tokyo 104-0045, Japan*
[2]*Department of Cardiovascular Science and Medicine, Chiba University Graduate School of Medicine, Chiba 260-8677, Japan*

Myo18B is an unconventional myosin family protein expressed predominantly in muscle cells. Although conventional myosins are known to be localized on the A-bands and function as a molecular motor for muscle contraction, Myo18B protein was localized on the Z-lines of myofibrils in striated muscles. Like Myo18A, another 18th class of myosin, the N-terminal unique domain of the protein and not the motor domain and the coiled-coil tail is critical for its localization to F-actin in myocytes. Myo18B expression was induced by myogenic differentiation through the binding of myocyte-specific enhancer factor-2 to its promoter. Deficiency of Myo18B caused an embryonic lethality in mice accompanied by disruption of myofibrillar structures in cardiac myocytes at embryonic day 10.5. Thus, Myo18B is a unique unconventional myosin that is predominantly expressed in myocytes and whose expression is essential for the development and/or maintenance of myofibrillar structure.

Introduction

Myosins constitute a large superfamily of actin-based motor proteins that use ATP to play fundamental roles in many forms of eukaryotic cell motility, such as cell migration, cytokinesis, phagocytosis, and trafficking. A total of 40 myosin genes have been identified in humans to date; however, physiological and biological functions of more than half of their products are still unknown. (Mermall *et al.* 1998; Wu *et al.* 2000; Berg *et al.* 2001). We previously isolated a novel unconventional myosin, MYO18B, from a homozygously deleted region at chromosome 22q12.1 in a human lung cancer cell line (Nishioka *et al.* 2002). Inactivation of this gene by genetic and/or epigenetic alterations in human cancer cells suggests that the *MYO18B* gene functions as a tumor suppressor in human carcinogenesis (Nishioka *et al.* 2002; Tani *et al.* 2004; Yanaihara *et al.* 2004; Nakano *et al.* 2005). Like other myosins, MYO18B has a myosin head motor domain with an ATP-binding motif and a GPA actin-binding motif. It also contains a neck region with an IQ motif that is thought to participate in binding to myosin light chains or calmodulin and a C-terminal tail with a coiled-coil domain that likely mediates dimer formation. Furthermore, MYO18B has unique N- and C-terminal extensions (Fig. 1A), which should give a distinction against other classes of myosins. However, physiological functions of MYO18B are largely unknown. Here, we showed the N-terminal unique domain of MYO18B is crucial for its localization to F-actin, and analysis of *Myo18B* gene targeted mice revealed that Myo18B protein is crucial for the development and/or maintenance of myofibrillar structure in myocytes.

Communicated by: Fuyuki Ishikawa
**Correspondence*: jyokota@gan2.ncc.go.jp
[a]Current address: Cell and Developmental Biology Laboratory, National Cancer Institute-Frederick, NIH, MD 21702, USA.

Results

Contribution of N-terminal extension of Myo18B protein to its localization on F-actin

To characterize the functions of Myo18B, we used C2C12 cells because the *Myo18B* transcription is increased by myogenic differentiation in C2C12 mouse myoblast cells (Salamon *et al.* 2003). Western blot analysis reveals that endogenous Myo18B protein level increases along with C2C12 cells differentiation (Fig. 1B). Then, we carried out immunofluorescence analysis of C2C12 cells using two independent antibodies against Myo18B. Endogenous Myo18B protein stained very faintly in undifferentiated C2C12 cells, but better in multinucleated differentiated

DOI: 10.1111/j.1365-2443.2008.01226.x
© 2008 The Authors
Journal compilation © 2008 by the Molecular Biology Society of Japan/Blackwell Publishing Ltd.

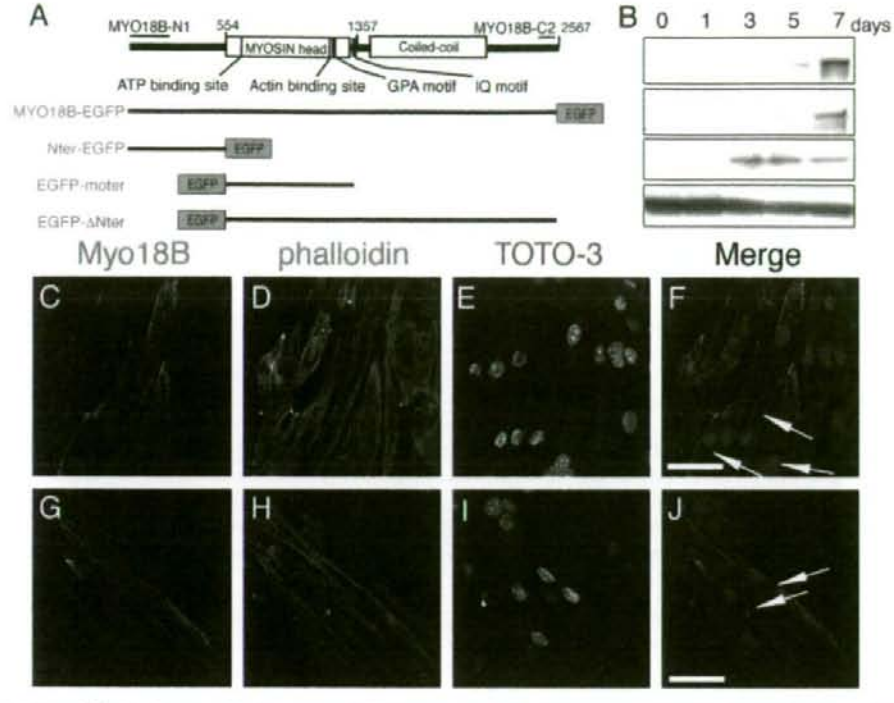

Figure 1 Intracellular localization of endogenous and deletion mutants of Myo18B protein in C2C12 cells. (A) Structure of MYO18B protein, positions of antigens for antibodies and EGFP-fusion protein structures used below are shown. (B) Western blot analysis of C2C12 cells with induction of myogenic differentiation using antibodies, anti-MYO18B-N1 (upper panel), anti-MYO18B-C2 (upper middle panel), anti-Myogenin (lower middle panel), and anti-α tubulin (lower panel). Confocal images of immunocytochemistry of differentiated C2C12 cells (C–J) using anti-MYO18B-N1 (C and green in F) and anti-MYO18B-C2 (G and green in J) are shown. Arrows in F and J indicate differentiated and multinucleated C2C12 cells. Localization of EGFP-fusion deletion mutants of MYO18B is shown (K–Z). MYO18B-EGFP (K–N), Nter-EGFP (O–R), EGFP-moter (S–V) and EGFP-ΔNter (W–Z) were expressed in C2C12 cells. The cells were co-stained with phalloidin (D, H, L, P, T, X and red in F, J, N, R, V, Z) and TOTO-3 (E, I, M, Q, U, Y and blue in F, J, N, R, V, Z). Bars = 50 μm (F), 20 μm (J, N, R, V, Z).

C2C12 cells that were positive for myoglobin and skeletal myosin (data not shown). This result is consistent with the result of Western blot analysis. In differentiated C2C12 cells, Myo18B was predominantly distributed on F-actin with a punctate pattern (Fig. 1C–J). Previously Myo18B protein was reported to be localized in the nucleus of differentiated C2C12 cells and striated muscles (Salamon *et al.* 2003); however, the antibodies did not indicate a nuclear distribution of Myo18B protein in both differentiated C2C12 cells and striated muscles.

To reveal which domain of Myo18B contributes to the localization on F-actin, we prepared expression vectors for EGFP-fused MYO18B full-length (MYO18B-EGFP) protein and for deletion mutants (Fig. 1A). Exogenously expressed MYO18B-EGFP in C2C12 cells was predominantly distributed on actin stress fibers as endogenous Myo18B, and localized in cytoplasm with a punctate pattern (Fig. 1K–N). When cells had a protruded region, which is a region where F-actin is actively polymerized, MYO18B-EGFP co-localized to these sites as well (data not shown) consistent with results shown previously in NIH3T3 cells (Ajima *et al.* 2007). Analysis of an EGFP-fused N-terminal half (1–1357 a.a.) and C-terminal half (1357–2567 a.a.) of MYO18B protein revealed that the N-terminal half of MYO18B is necessary, but dimerization with a coiled-coil domain in the C-terminal half of MYO18B, is not necessary for localization on F-actin (data not shown). The N-terminal half of MYO18B was

© 2008 The Authors
Journal compilation © 2008 by the Molecular Biology Society of Japan/Blackwell Publishing Ltd.

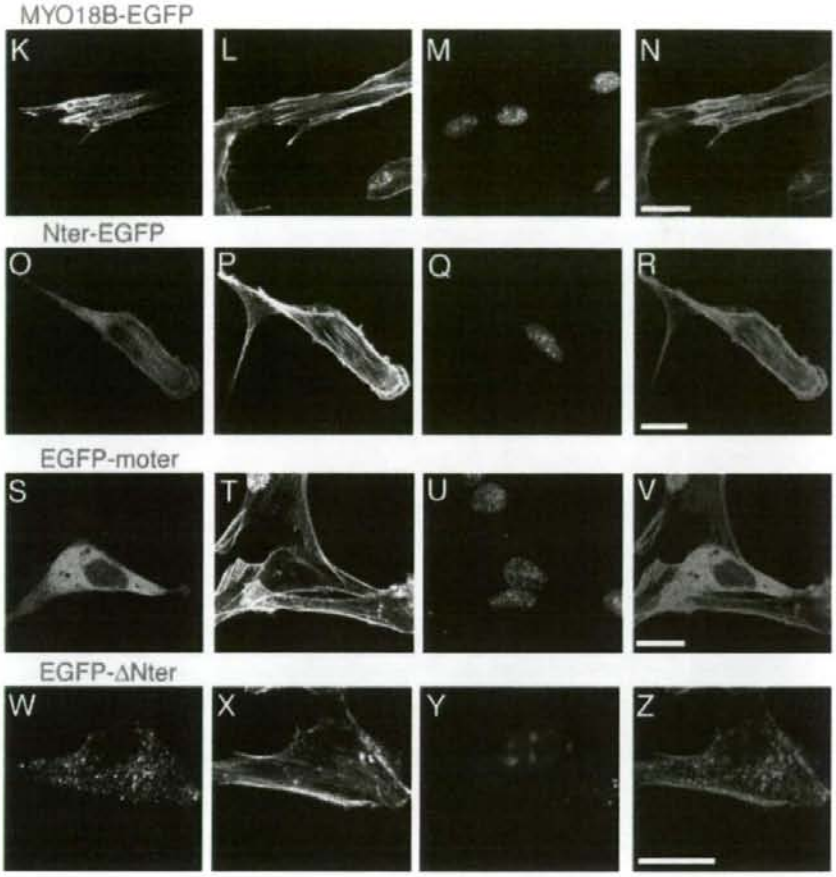

Figure 1 *Continued*

further divided into the N-terminal extension (Nter-EGFP) and the motor region (EGFP-moter) and both were expressed in C2C12 cells. EGFP-moter was homogenously distributed throughout the cytoplasm (Fig. 1S–V), whereas Nter-EGFP was localized clearly on F-actin (Fig. 1O–R). A vector of MYO18B without the N-terminal extension (EGFP-ΔNter) was also expressed. EGFP-ΔNter was localized in the cytoplasm with a punctate pattern as MYO18B-EGFP, but its localization on actin stress fibers was unclear (Fig. 1W–Z). Taking these results together, it was concluded that the N-terminal extension of MYO18B protein greatly contributes to the localization of MYO18B on actin stress fibers.

Intracellular localization of Myo18B protein in striated muscle cells

To reveal the localization of Myo18B protein in skeletal and cardiac muscles, we carried out immunohistochemistry using anti-MYO18B antibodies. Myo18B showed a stripe pattern in muscle cells, suggesting that Myo18B is localized in either the A-bands or the Z-lines. The cells were co-stained with an α-actinin antibody, a marker of the Z-lines. α-actinin showed a stripe pattern in the same region, but the bands for α-actinin were thinner and sharper than those for Myo18B. The result indicated that Myo18B is localized in the Z-lines and in the

© 2008 The Authors
Journal compilation © 2008 by the Molecular Biology Society of Japan/Blackwell Publishing Ltd.

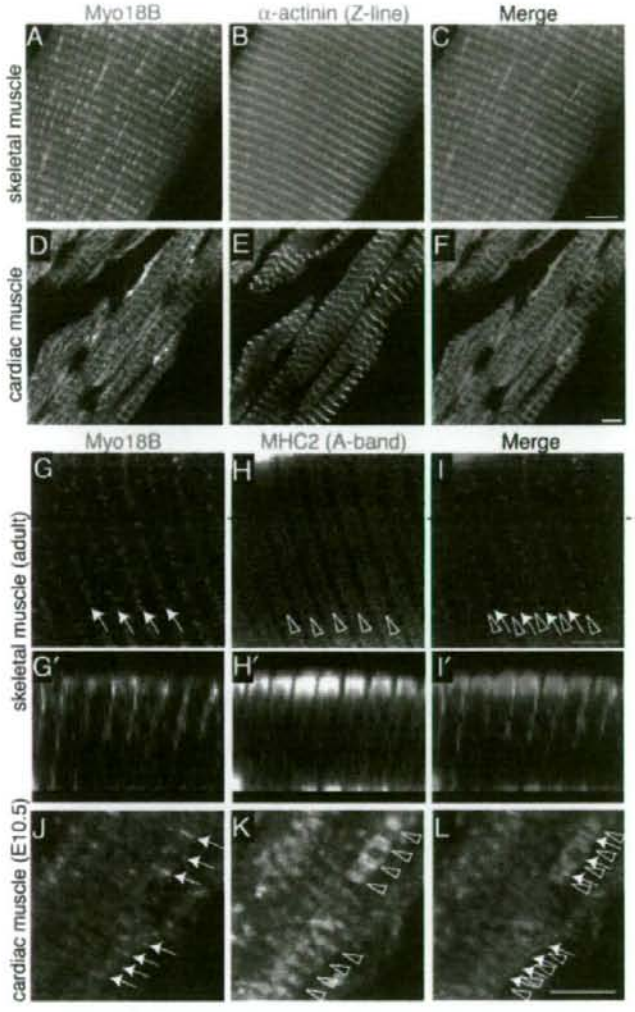

Figure 2 Intracellular localization of endogenous Myo18B protein in striated muscles. Confocal images of frozen sections of skeletal muscle (A, B, C and G, G′, H, H′, I, I′), cardiac muscle (D, E, F) of adult mice and sections of paraffin embedded cardiac muscle of an E10.5 embryo (J, K, L) that are immunohistochemically stained with anti-MYO18B-N1 (A, D, G, G′, J and green in C, F, I, I′, L), anti-α-actinin (B, E and red in C, F), anti-skeletal myosin (H, H′ and red in I, I′) and anti-myosin heavy chain β (K and red in L) antibodies are shown. The localization of Myo18B is indicated by arrows and that of the A-bands is indicated by triangles (G–L). X–Z scan at the doted line in G, H, I, along the longitudinal axes of myocytes are shown in G′, H′, I′. Bars = 5 μm.

region adjacent to the Z-lines in both skeletal and cardiac muscles (Fig. 2A,B,C and D,E,F). Co-staining of Myo18B with type II myosin showed that Myo18B did not co-localize with type II myosin in adult skeletal muscles (Fig. 2G,G′,H,H′,I,I′) or in cardiac muscles of E10.5 wild-type embryos, either (Fig. 2J,K,L). A confocal X-Z scan image confirmed that Myo18B was localized in myofibrils between the A-bands (Fig. 2G′,H′,I′). These results suggest that Myo18B is not used as a molecular motor in the A-bands for muscle contraction and plays a distinct role from conventional myosins.

Regulation of Myo18B expression in myogenic differentiation of C2C12 mouse myoblast cells

Because Myo18B protein is induced by myogenic differentiation, Myo18B gene expression could be strictly regulated by myogenic transcriptional factors. To analyze the transcriptional regulation of the *Myo18B* gene, we

© 2008 The Authors
Journal compilation © 2008 by the Molecular Biology Society of Japan/Blackwell Publishing Ltd.

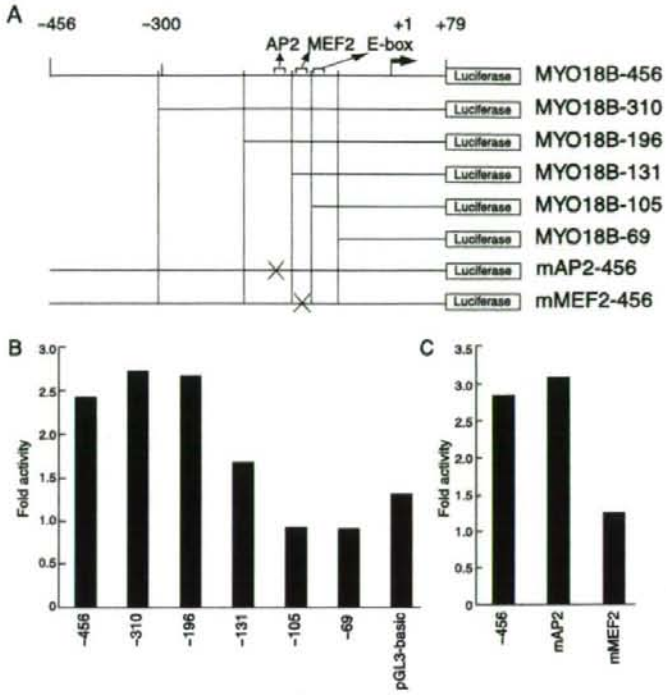

Figure 3 Regulation of Myo18B expression during differentiation of C2C12 myoblasts. (A) Schematic representation of the *MYO18B* gene promoter region and deletion constructs. The positions of transcriptional factor-response elements that are conserved in humans and mice and the position of the transcriptional start site (+1) are shown above a wild type *MYO18B* promoter construct, MYO18B-456. (B and C) Fold luciferase activities of several *MYO18B* promoter constructs compare with undifferentiated and differentiated C2C12 cells. The luciferase activities of MYO18B-456, six promoter deletion constructs (-310, -196, -131, -105, and -69 in B), and mutant constructs for AP2 and MEF2 responsible elements (mAP2 and mMEF2, respectively in C) in C2C12 cells were determined by transfecting the cells with each construct. Fold activities were calculated by dividing differentiated C2C12 cells activity with undifferentiated C2C12 cells activity. Constructs were used more than 3 times and showed similar results.

compared the genomic structure in the 5′ region of the human *MYO18B* and mouse *Myo18B* genes using the ClustalW multiple sequence alignment program (http://align.genome.jp/). The nucleotide sequence between the -350 nucleotide and a putative transcription start site (+1) of the human gene was highly conserved in the mouse gene. Furthermore, we screened repetitive elements upstream of the promoter region of the *Myo18B* gene using the RepeatMasker program (http://www.repeatmasker.org). Repetitive elements started roughly 500 nucleotides upstream from the putative transcription start site (Fig. 3A). Therefore, to define the critical elements for regulation of Myo18B mRNA expression in myocytes and during their differentiation, a series of *MYO18B* promoter deletion constructs were cloned with reporter vectors for the luciferase assay (Fig. 3A). These vectors were introduced into C2C12 cells and the differentiation was induced. The MYO18B-456 promoter activity in differentiated C2C12 cells was 2–3 times higher than that in undifferentiated cells. The induction of promoter activity was kept with MYO18B-310 and MYO18B-196 constructs, but was decreased with the MYO18B-131 construct and diminished with MYO18B-105 or -69 constructs (Fig. 3B). So, the segments of nucleotides -196 to -131 and -131 to -105 of the *MYO18B* gene were suggested to bear an enhancer element for myocyte differentiation. A putative AP2-response element was present between nucleotides -196 and -131, and an AT-rich putative MEF2-response element was between nucleotides -131 and -105, and both element were conserved in human and mouse (Fig. 3A). Therefore, reporter vectors with a mutation in each putative binding site of the *MYO18B* promoter were further constructed. A reporter construct with a mutation in the putative AP2-response element showed similar promoter activity as MYO18B-456 promoter. In contrast, a reporter construct with a mutation in the putative MEF2-response element showed slight induction by myogenic differentiation (Fig. 3C). These results suggest that MEF2 plays an important role in the induction of Myo18B expression in myocytes.

Generation of Myo18B gene targeting mice and embryonic lethality of homozygous knockouts

A targeting vector was constructed by insertion of the bacterial *nls-LacZ* and *NeoR* genes into exon 2 containing

© 2008 The Authors
Journal compilation © 2008 by the Molecular Biology Society of Japan/Blackwell Publishing Ltd.

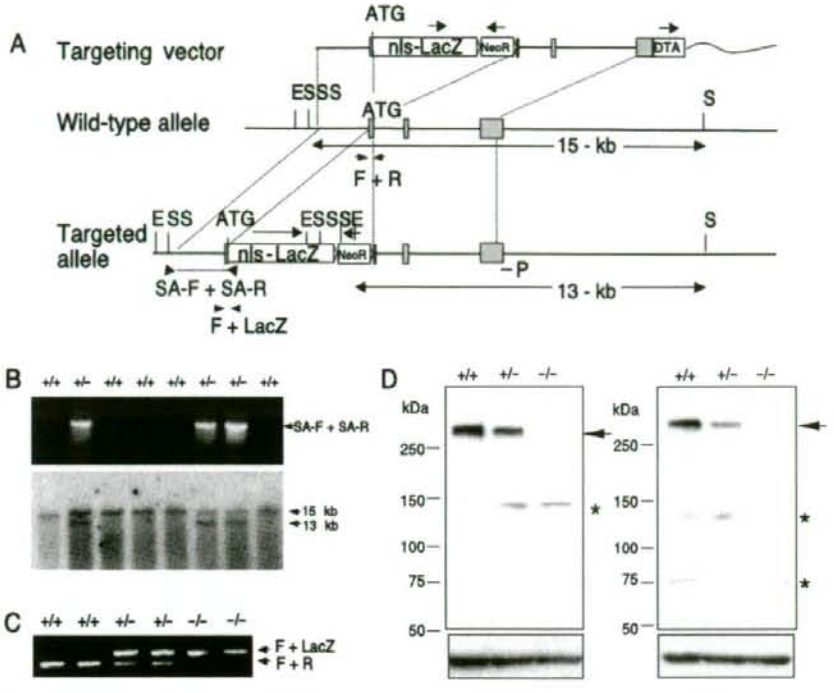

Figure 4 Targeted disruption of the mouse *Myo18B* gene and its expression. (A) Targeting strategy with the targeting vector (*top*), a restriction map of the wild-type *Myo18B* allele covering exon 2 to exon 4 (*middle*), and the targeted allele disrupted by a homologous recombination (*bottom*) are shown. ATG, SA-F + SA-R; PCR primer sets for ES screening and genotyping for short arm, F + R; PCR primer sets for genotyping wild-type allele, and F + LacZ; PCR primer sets for genotyping targeted allele, P; probe for Southern blot analysis, and 15-kb/13-kb of the expected fragment lengths are indicated. E, *EcoRI*; S, *SphI*; *nls-LacZ*; nuclear localization signal-*β-galactosidase* gene, *NeoR*; neomycin resistant gene, *DTA*; *Diphtheria toxin A* gene. Arrows above gene cassettes indicate the direction of the genes. (B) Representative results of PCR and Southern blot analyses for genotyping of ES cells and F1 mice are shown. The 2.2-kb PCR fragments represent a disrupted allele (upper), and 15 kb and 13 kb *EcoRI*/*SphI* genomic DNA fragments represent the wild-type and the disrupted alleles, respectively (lower). (C) Representative results of PCR-mediated genotyping of embryos are shown. The primers are shown by arrows in A. +/+, *Myo18*$^{+/+}$; +/−, *Myo18*$^{+/-}$; and −/−, *Myo18*$^{-/-}$. (D) Results of Western blot analysis for Myo18B protein in cultured whole embryo are shown. Upper left and right panels are blots by anti-MYO18B-N1 and anti-MYO18B-C2 antibodies, respectively. Both lower panels are blots by anti α-tubulin antibody. Myo18B protein is indicated by arrows, and non-specific bands are indicated by*.

the translation initiation codon of the mouse *Myo18B* gene (Fig. 4A). Two independent *Myo18*$^{+/-}$ ES cell clones, 109 and 153, were established, used to make *Myo18* mutant chimeric and heterozygous mice. Targeting disruption of the gene in ES clones and heterozygous mice was confirmed by PCR and Southern blot analyses (Fig. 4B). The mice appeared healthy and fertile, with no indication of physical abnormalities.

Heterozygous mice were then mated to obtain mice with Myo18B deficiency. However, no live *Myo18B*$^{-/-}$ offspring was born from either line, implying that *Myo18B*$^{-/-}$ embryos had died during embryogenesis. To determine the time of death, embryos from different developmental stages were genotyped by PCR (Fig. 4C) and macroscopically inspected (Table 1). Up to E10, the expected Mendelian ratio of viable *Myo18B*$^{-/-}$ embryos was observed. However, at E10.5 to E11, 12 of 31 *Myo18B*$^{-/-}$ embryos were abnormal and 4 empty deciduas were observed. At E11.5 to E13.5, none of the remaining 9 *Myo18B*$^{-/-}$ embryos were normal and the number of empty deciduas increased. *Myo18B*$^{-/-}$ dead embryos were shown to have either dilated pericardial cavities, internal hemorrhage or resorption.

© 2008 The Authors
Journal compilation © 2008 by the Molecular Biology Society of Japan/Blackwell Publishing Ltd.

Table 1 Genotypes and phenotypes of Myo18B heterozygous intercrosses

		Total	*Myo18B*$^{+/+}$	*Myo18B*$^{+/-}$	*Myo18B*$^{-/-}$ (D/V)*	Empty decidua	Aspects of *Myo18B*$^{-/-}$ dead embryos†
Newborn	line 153	112	50	62	0		
	line 109	107	40	67	0		
Embryo (line 153)	E11.5–13.5	55	14	24	9 (9/0)	8	1D; 1H; 7R
	E10.5–11	139	37	67	31 (12/19)	4	1D; 7H; 4R
	E9.5–10	74	13	37	19 (0/19)	0	

*The number of dead (D) and viable (V) embryos is shown as D/V in parentheses.
†The number of Myo18B dead embryos with dilated pericardiac cavity (D), internal hemorrhage (H), and resorption (R) is shown.

To verify the knockout of the targeted region, Western blot analysis with lysates of cultured whole embryos (Fig. 4D) were carried out. A prominent 290-kD band was detected in the lysate of wild-type (*Myo18B*$^{+/+}$) embryos. The intensity of the band decreased in *Myo18B*$^{+/-}$ embryos, and the band disappeared in *Myo18B*$^{-/-}$ embryos.

Myo18B expression probed by the knocked-in bacterial LacZ gene in *Myo18*$^{+/-}$ mice

β-Galactosidase, the gene product of *nls-LacZ*, generates blue signals by hydrolyzing X-Gal. Therefore, the knocked-in *nls-LacZ* gene under the transcriptional control of the endogenous *Myo18B* promoter signals the pattern of *Myo18B* mRNA expression in *Myo18*$^{+/-}$ embryos and mice. The whole mount X-Gal staining of *Myo18*$^{+/-}$ embryos revealed that *nls-LacZ* was expressed in heart and somites at E9.5 and E11.5 (Fig. 5A–C). At E13.5, *nls-LacZ* expression was prominent in muscles of the cardiac atriums and ventricles (Fig. 5D left and lower right panel), and was also detected in myotomes and muscle mass (Fig. 5D left and upper right panel). In *Myo18*$^{+/-}$ adult mice, *nls-LacZ* was expressed prominently in cardiac and skeletal muscles (Fig. 5E,F) as well as in smooth muscles of several tissues, and in some parts of testis and brain (data not shown). The pattern of Myo18B expression indicated by X-gal staining was similar to that previously shown by tissue Northern blot analysis (Salamon *et al.* 2003).

Cardiac defects in *Myo18B*$^{-/-}$ embryos

Macroscopically, the *Myo18B*$^{-/-}$ embryos appeared to be normal in early developmental stages, with no detectable abnormality up to E9.5. Abnormal embryos were found as early as E10.5. From E10.5 to E13.5, the number of resorbed or growth-retarded embryos (Fig. 6D) increased, and some unresorbed *Myo18B*$^{-/-}$ embryos showed severe internal hemorrhage in the cardiac and ventral body wall regions (Fig. 6B) or pericardiac cavity dilation (Fig. 6H).

Therefore, *Myo18B*$^{-/-}$ embryos and control (*Myo18B*$^{+/+}$ and *Myo18B*$^{+/-}$ embryos) littermates were histologically analyzed at various developmental stages. At E9.5, *Myo18B*$^{-/-}$ embryos showed a normal looping of the linear heart tube and correct cardiac morphology compared with control embryos (data not shown). At E10.5, the formation of the cardiac chambers was initiated correctly in *Myo18B*$^{-/-}$ embryos that were neither resorbed nor hemorrhagic. However, some *Myo18B*$^{-/-}$ embryos at E10.5 to E12.5 showed striking abnormalities in the myocardium (Fig. 6F,H). Variable degrees of pericardial effusion were observed (Fig. 6H). The lumens of both the right and left cardinal veins and the right atrium in *Myo18B*$^{-/-}$ embryos were morbidly enlarged (Fig. 6F,H) when compared with controls (Fig. 6E,G).

Abnormal myofibrillar organization in *Myo18B*$^{-/-}$ cardiac myocytes

Ultrastructural analysis of comparable areas from the left ventricular free walls of *Myo18B*$^{+/+}$ and *Myo18B*$^{-/-}$ embryos revealed abnormalities in sarcomeric assembly in the *Myo18B*$^{-/-}$ embryos. *Myo18B*$^{-/-}$ cardiac myocytes had normal sarcomeres length with structures of intercalated disks and Z-lines, but displayed a disorganized alignment of parallel thick and thin filaments (Fig. 7B,C) when compared with *Myo18B*$^{+/+}$ cardiac myocytes (Fig. 7A). Additionally, in transverse sections of myofibrils, *Myo18B*$^{+/+}$ myocytes showed ordered alignment of thick filaments and of thin filaments surrounding thick filaments (Fig. 7D,D′); however, *Myo18B*$^{-/-}$ myocytes showed disordered alignment and unbalanced distribution of thick and thin filaments (Fig. 7E,E′,F,F′). These data indicate that Myo18B is necessary for the development and/or maintenance of normal cardiac myofibril structure.

© 2008 The Authors
Journal compilation © 2008 by the Molecular Biology Society of Japan/Blackwell Publishing Ltd.

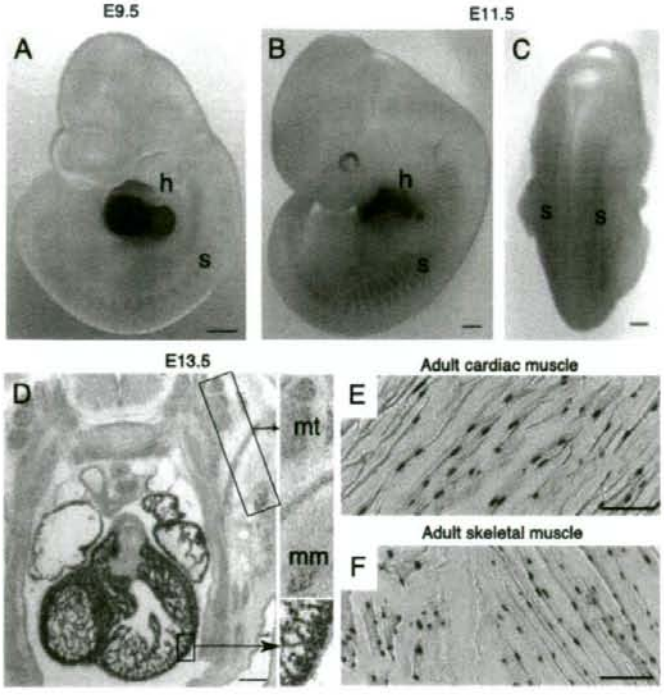

Figure 5 Myo18B expression probed by LacZ after X-Gal staining. Whole-mount staining of E9.5 (A) and E11.5 (B, C) *Myo18*$^{+/-}$ embryos. Staining of cross sections at the level of the forelimb (D) of an E13.5 *Myo18*$^{+/-}$ embryo. High magnification view of the boxed regions is shown in right panels. Staining of sections of cardiac (E) and skeletal muscle (F) of an adult *Myo18*$^{+/-}$ mouse. Bars = 1 mm (A–C), 0.2 mm (D), 0.1 mm (E, F). Abbreviations: h, heart; s, somites; mt, myotome; mm, muscle mass.

Discussion

We demonstrated here that Myo18B is a unique unconventional myosin that is predominantly expressed in cardiac and skeletal muscle cells and its expression is essential for the development and/or maintenance of myofibrillar structure in myocytes. Most unconventional myosins are known to be expressed ubiquitously in various types of cells, or specifically in non-muscle cells, such as MYO15A (Liang *et al.* 1999). Thus, Myo18B is a unique unconventional myosin that is predominantly expressed in myocytes like conventional (type II) myosins. Whereas conventional myosins, which consist of 15 genes in humans, are expressed in a time limited manner in specific types of myocytes, Myo18B is expressed in cardiac, skeletal and a part of smooth muscle cells, and is expressed from the embryonic stage to adulthood. Therefore, the expression pattern of Myo18B is distinct from conventional myosins. Promoter analyses of the *Myo18B* gene revealed that MEF2 plays an important role in *Myo18B* gene expression in myocytes. The expression patterns of the *MEF2* genes *in vivo* are very similar to that of the *Myo18B* gene (Edmondson *et al.* 1994). These data support the regulation of *Myo18B* gene expression by MEF2.

Another unique aspect of Myo18B is its localization to the Z-lines and their peripheral regions in striated muscle cells, because most conventional myosins are localized to the A-bands. One member of conventional myosins, non-muscle myosin IIB (NMHCIIB), is also localized to the Z-lines in cardiac myocytes (Takeda *et al.* 2000). *NMHCIIB* deficiency in mice showed cardiac myocyte enlargement and binucleation (Tullio *et al.* 1997; Uren *et al.* 2000; Takeda *et al.* 2003). This phenotype is clearly different from the phenotype of *Myo18B* deficiency. Thus, physiological functions of these two myosins are likely to be distinct from each other. Because the N-terminal extension of Myo18B was localized on stress fiber, Myo18B is likely to interact with F-actin through not only the motor domain but also the N-terminal unique extension. Recently, MYO18A, another 18th class of myosin, was shown to be localized on F-actin with the domain of its N-terminal extension. The residues in the N-terminal extension that are conserved between MYO18A and MYO18B were further shown to be important for the physiological interaction of MYO18A to F-actin

© 2008 The Authors
Journal compilation © 2008 by the Molecular Biology Society of Japan/Blackwell Publishing Ltd.

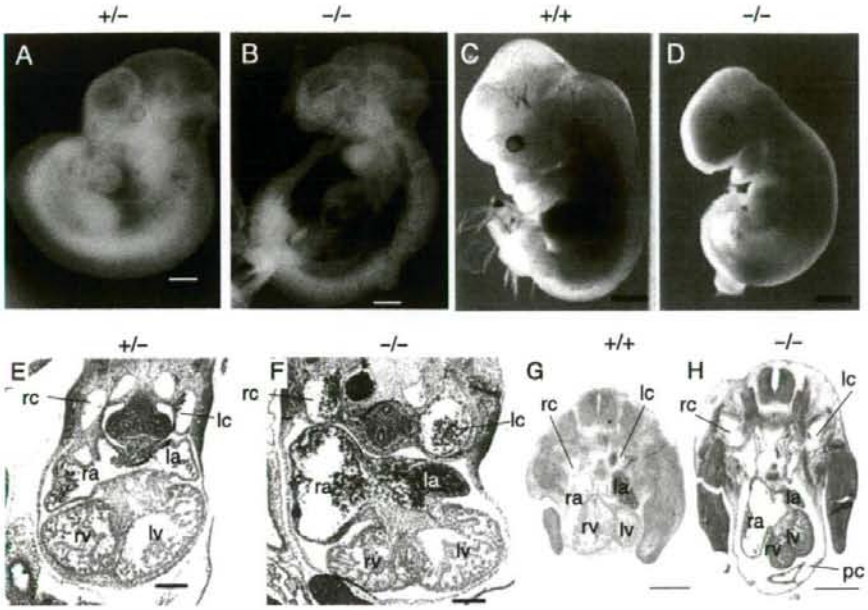

Figure 6 Analysis of embryonic development in control and Myo18B mutant embryos. (A–D) Control (A, C) and *Myo18*$^{-/-}$ embryos (B, D) at E10.5 and E12.5 are shown. *Myo18*$^{-/-}$ embryos displayed an internal hemorrhage at E10.5 (B) and were resorbed at E12.5 (D). (E–H) Comparative histological analysis of heart structures in control and *Myo18*$^{-/-}$ embryos at E10.5 and E12.5. Mid-level sections from control (E, G) and *Myo18*$^{-/-}$ hearts (F, H) are shown. *Myo18*$^{-/-}$ embryos show a cardinal veinal and atrial enlargement (F, H) and dilated pericardiac cavity (H) compared with control (E, G). Myo18B-153 line mice were used for all the data in this figure. Abbreviations: rc, right cardinal vein; lc, left cardinal vein; ra, right atrium; la, left atrium; rv, right ventricle; lv, left ventricle; pc, pericardiac cavity. Bars = 0.1 mm (A, B, E, F), 1 mm (C, D), 0.5 mm (G, H).

(Isogawa *et al.* 2005). This data also support the possibility that Myo18B interacts with F-actin through its N-terminal unique extension. However, Myo18B did not localize along with thin filaments in striated muscle cells (Fig. 2), and localized on stress fiber with a punctuated structure (Fig. 1). Furthermore, our previous study showed that Myo18B is localized in the region of membrane protrusion, but not of cell-cell contact, although both regions are known as ones with F-actin rich structure (Ajima *et al.* 2007). These results strongly indicate that Myo18B does not co-localize with F-actin itself, but co-localize with some actin-associated proteins, which are present in stress fibers or in the region surrounding the Z-lines.

Myo18B$^{-/-}$ embryos were lethal during embryogenesis, and dead embryos had either dilated pericardial cavities or internal hemorrhage. Furthermore, cardiac myofibrillar aberrations were observed in *Myo18B*$^{-/-}$ myocytes. Therefore, it is likely that Myo18B functions in the Z-lines during the development and/or maintenance of highly ordered structures of thick and thin filaments, and that this function of Myo18B cannot be compensated for by other myosins *in vivo*. Such myofibril aberrations in *Myo18B*$^{-/-}$ myocytes could lead to their reduced contractility that results in the occurrence of heart failure and embryonal death at E10.5–11.5 of *Myo18B*$^{-/-}$ embryos. However, whether or not cardiac myofibrillar disorganization in *Myo18B*$^{-/-}$ embryos disrupts cardiac myocyte function and leads embryonic lethality remains to be clarified, because pericardial effusion could occur not only by myocardial dysfunction itself but also by several other circulation defects. Therefore, to resolve this question, further functional studies of *Myo18B*$^{-/-}$ myocytes will be needed.

The Z-lines and the region adjacent to the Z-lines, where Myo18B locates, is known to be important not only to keep the structure of the sarcomeres but also to regulate the function of striated muscles. Protein complexes

© 2008 The Authors
Journal compilation © 2008 by the Molecular Biology Society of Japan/Blackwell Publishing Ltd.

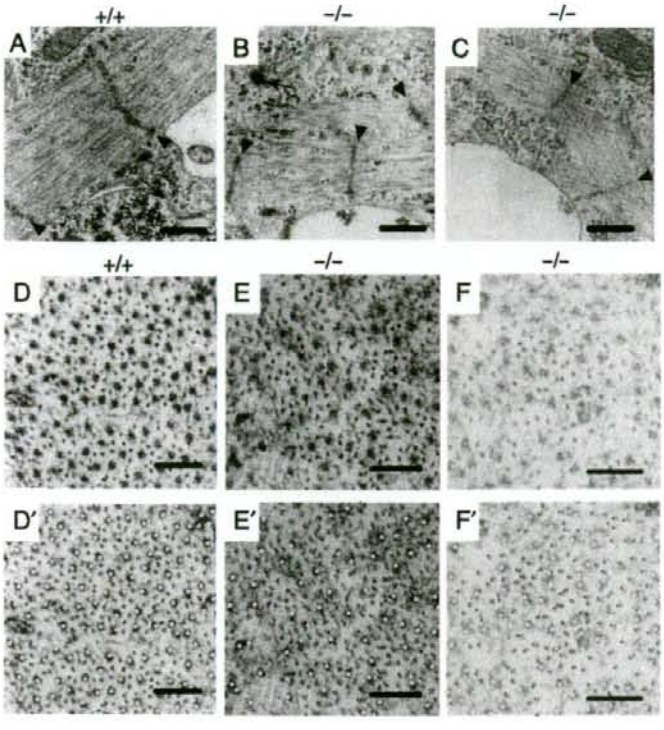

Figure 7 Ultrastructural analysis of cardiac myocytes by TEM. Representative images were taken from comparable areas of ventricular free walls. Vertical sections (A, B, C) and transverse sections (D, E, F) of myofibrils of E10.5 *Myo18*$^{+/+}$ (A, D) and *Myo18*$^{-/-}$ (B, C, E, F) embryos are shown. Arrows and arrowheads indicate intercalated disk and Z-line, respectively. Thick filaments and thin filaments are marked in yellow and red dots, respectively (D′, E′, F′) in the same fields of D, E, and F. Bars = 0.5 μm (A–C), 0.1 μm (D–F).

in the peripheral region of the Z-lines physically interact with costameres, which transmit contractile forces from the sarcomere across the sarcolemma to the extracellular matrix, and mutations of genes for several proteins in these protein complexes cause diseases of muscle (Reviewed in Ervasti 2003; Frank *et al.* 2006). For instance, germline mutations of genes encoding cardiac α-actin, muscle LIM-domain protein (MLP), desmin and Cypher/Z ASP have been found in patients with familial dilated cardiomyopathy (Chien 2000; Knoll *et al.* 2002; Mohapatra *et al.* 2003; Arimura *et al.* 2004). Mice deficient in these genes, which are considered as being models of human dilated cardiomyopathy, resulted in the formation of disordered myofibrillar structures (Milner *et al.* 1996; Arber *et al.* 1997; Honda *et al.* 1998; Zhou *et al.* 2001; Chu *et al.* 2003; Abdelwahid *et al.* 2004). Thus, these proteins in the Z-lines could also be essential for the development and/or maintenance of highly ordered myofibrillar structures in cardiac myocytes, and their defects may induce dilated cardiomyopathy. The phenotypes of Myo18B deficient mice, such as enlargement of the right atrium and disordered myofibrillar structures, are similar to dilated cardiomyopathy developed in these model mice. Therefore, functional and physiological interaction of Myo18B with these proteins will help us further elucidate the function of Myo18B in myocytes and clarify the molecular mechanism of the onset of dilated cardiomyopathy. It will be also worth investigating whether germline *MYO18B* mutations are present in a subset of familial dilated cardiomyopathy.

Experimental procedures

Preparation of anti-Myo18B antibody

Glutathione *S*-transferase (GST)-MYO18B C-terminal (human MYO18B 2448–2518 a.a. region) fusion protein was produced from pGEX-6T (Amersham Pharmacia Biotech), and recombinant protein was isolated by a glutathione–Sepharose 4B column (Amersham Pharmacia Biotech), cleaved by 150 U/mL PreScission Protease (Amersham Pharmacia Biotech), and were used to immunize two rabbits. Antisera from the immunized rabbits were affinity

© 2008 The Authors
Journal compilation © 2008 by the Molecular Biology Society of Japan/Blackwell Publishing Ltd.

purified using the antigenic column, and immunoabsorbed against GST and *E. coli* proteins. Polyclonal antibody (pAb) against MYO18B C-terminal proteins was designated as anti-MYO18B-C2.

Western blot analysis

Cells were lysed with TNE buffer [10 mM Tris-Hcl (ph7.5), 150 mM NaCl, 1 mM EDTA, 1% NP-40 and complete Mini protease inhibitor tablet (Roche)], and lysates were resolved by SDS-PAGE and electroblotted to PVDF membranes (Millipore). The membranes were blocked with 0.05% Tween 20, 3% Skim milk in TBS. Anti-MYO18B-N1 (Ajima *et al.* 2007) and anti-MYO18B-C2 antibodies (1:2000) were used with anti-rabbit IgG-HRP (1:3000; Santa-Cruze Biothecnology). Monoclonal antibodies (mAbs) against myogenin (1:1000; Santa-Cruze Biotechnology) and α-tubulin (1:10 000; Sigma-Aldrich) were used with anti-mouse IgG-HRP (1:3000; Santa-Cruz Biotechnology). Bands were detected by chemiluminescence (PIERCE).

Vector construction

For reporter vector construction, the 5′ region (−456 to +79) of the human *MYO18B* gene was amplified by PCR and ligated into the pGL3 basic vector (Promega). Deletion constructs were generated from MYO18B-456 (−456 to +79) by serial deletions of the 5′ end by restriction enzyme digestion. Namely, the MYO18B-456 fragment in the vector was digested with *FauI, NcoI, SacI, SalI, XomI*, and *SmaI/HindIII* to produce MYO18B-310 (−310 to +79), MYO18-196 (−196 to +79), MYO18-131 (−131 to +79), MYO18-105 (−105 to +79), and MYO18-69 (−69 to +79), respectively. Deletion constructs were then ligated into the corresponding restriction sites in the multiple cloning sites of the vector. To produce a construct with a mutation in the putative AP2- or MEF2-binding site, a site-directed mutagenic PCR was carried out with primer sets, mAP2 Forward (5′-GCTGCCG TCT*ACTGACCAGATCTGGATC*TC ACAAGCTAAT-3′) and mAP2 Reverse (5′-ATTAGCTTGTGA*GATCCAGATCTGGT* CAGTAGACGGCAGC-3′), or mMEF2 Forward (5′-GACCTGG AGCTCACAAG*CTGACGTTCGAAA*TGACTGGTCGACTC-3′) and mMEF2 Reverse (5′-GAGTCGACCAGTCA*TTTCGA ACGTCAG*CTTGTGAGCTCCAGGTC-3′), using a QuickChangeTM Site-directed Mutagenesis Kit (Stratagene). Positions of the binding sites are underlined, and mutated nucleotides are indicated in italics.

For the construction of an EGFP-fusion full-length MYO18B expression vector, the stop codon of human *MYO18B* cDNA in the pcDNA3.1+ vector (Nishioka *et al.* 2002) was excluded by a PCR based method, and *EGFP* cDNA from the pEGFP-N3 vector (BD Clontech) was inserted into the 3′ end of *MYO18B* cDNA. For the construction of an Nter-EGFP expression vector, the 1–554 a.a. region of MYO18B cDNA was amplified by PCR and inserted into the pEGFP-N3 vector (BD Clontech). For the construction of an EGFP-moter expression vector, the 555–1357 a.a. region of MYO18B cDNA was amplified by PCR and inserted into the pEGFP-C1 vector (BD Clontech). An EGFP-ΔNter expression vector was constructed by insertion of the 1357–2567 a.a. region of MYO18B cDNA from pcDNA3-MYO18B to the EGFP-moter vector.

Cell culture

C2C12 cells (ATCC) were cultured in DMEM supplemented with 15% FBS. To induce differentiation of C2C12 cells, the medium was replaced by DMEM supplemented with 2% horse serum and further changed every 2 days for 1 week. E9.5 whole embryos were suspended in 150 μL matrigel (BD Biosciences) and dropped to the center of 6 well dishes. After 30 min incubation at 37 °C, a drop of embryo in matrigel was covered with DMEM supplemented with 10% fetal bovine serum (FBS). After 1-week's culture, cells were collected with BD cell recovery solution (BD Biosciences).

Transfection and luciferase assay

For luciferase assay, C2C12 cells were plated at 5×10^4 cells/well onto a 12-well dish one day before transfection, and the differentiation was induced by changing the medium just before transfection. The cells were then transfected with 0.5 μg of each reporter vector construct using FuGene6 (Roche) triplicate for each constructs, harvested 60 h after transfection, and cell extracts were prepared using a standard procedure. The transfection efficiency was determined by co-transfection of 5 ng of the *Renilla* luciferase expression vector (Promega) under the β-actin promoter, and relative luciferase activity was calculated as recommended by the manufacturer.

For immunocytochemistry, C2C12 cells were plated onto coverslips one day before transfection, and transfected with each expression vector construct using FuGene6 (Roche).

Immunohistochemistry and immunocytochemistry

For immunohistochemistry, sections were prepared as follows. For frozen sections, tissues were fixed overnight with 1% paraformaldehyde (PFA) at 4°C, washed with ice-cold phosphate-buffered saline (PBS), equilibrated with 10, 20, 30% sucrose in PBS at 4°C, embedded in Tissue-Tek OCT compound, and frozen using dry ice. The tissues were then sectioned at 10 mm thickness, mounted on glass slides, post-fixed with 0.2% PFA/PBS for 10 min, and permeabilized by 0.2% Triton X-100/PBS for 10 min. For paraffin sections, embryos were fixed overnight with 10% neutralized formalin, dehydrated, embedded in paraffin, sectioned at 5 mm thickness, and mounted on glass slides. The sections were then stained using a VECTOR M. O. M. Immunodetection Kit or a VECTASTAIN Elite ABC kit (VECTOR Laboratories) according to the manufacturer's protocol. For immunocytochemistry, C2C12 cells on coverslips were fixed with 4% PFA/PBS for 10 min, permeabilized by 0.2% Triton X-100/PBS for 10 min, and blocked with 2% BSA in PBS. Antibodies and reagents used were as follows: anti-MYO18B-N1 and anti-MYO18B-C1 rabbit pAbs (1:200); anti-α-actin mouse mAb (1:800; Sigma-Aldrich, EA-53); anti-skeletal myosin mAb (1:2000; Sigma-Aldrich, MY-32); anti-myosin heavy chain β (1:300; CHEMICON);

© 2008 The Authors
Journal compilation © 2008 by the Molecular Biology Society of Japan/Blackwell Publishing Ltd.

Rhodamine-Phalloidin (1:100; Molecular Probe); Alexa Fluor 488 conjugate goat anti-rabbit IgG (1:500; Molecular Probe); Cy3 conjugate goat anti-mouse IgG (1:1000; Jackson ImmunoResearch); Alexa Fluor 546 conjugate streptavidin (1:500; Molecular Probe). Confocal images were obtained using a Carl-Zeiss Radiance2000 system.

Generation of Myo18B knockout mice

A 2.0-kb 5′ genomic fragment and a 5.2-kb 3′ fragment flanking exon 2 of the Myo18B gene were amplified by PCR from a mouse C57BL/6J BAC clone (Rosewell Park Cancer Institute) DNA, and linked to the *nlsLacZ* and *NeoR* genes at the 5′ and 3′ positions, respectively, in pBluescript SK + (Stratagene co.). A Poly-A signal sequence was inserted between the *nlsLacZ* and *NeoR* genes. The *Diphtheria toxin A* (DTA) gene was also linked to the 3′ end of the targeting cassette (Fig. 4A). The targeting construct was linearized and electroporated into cultured ES cells, and G418-resistant cell clones were screened for homologous recombination by PCR and Southern blot analyses. Two independent ES cell clones with heterozygous targeted disruption of the *Myo18B* gene (clones109 and 153) were injected into blastocysts of C57/BL6J mice, 3 days after their fertilization to create chimeric mice. The chimeric male mice and C57/BL6J female mice were used to generate $Myo18B^{+/-}$ mice. The $Myo18B^{+/-}$ mice were interbred to generate $Myo18B^{-/-}$ mice. The animal experiment protocols were approved by the Committee for Ethics in Animal Experimentation, and the experiments were conducted in accordance with the Guideline for Animal Experiments of the National Cancer Center.

Genotyping of Myo18B gene targeted mice

Genomic DNA was isolated from ES cells and mouse tails. Genotypes of ES cells were first determined by PCR with a set of primers (SA-F: 5′-TCAGCTGTCCTGGATTTCAATAT AAAGCTGAAGA-3′ and SA-R: 5′-TGCGCAACTGTTGGG AAGGGCGATC-3′) that specifically amplified the disrupted gene, and then confirmed by Southern blot analysis with a probe marked in Fig. 4A. Genotypes of offsprings were determined using tail or yolk sac DNA by PCR (primer sequences: F = 5′-GAGCACTCAGAAGCACAACGTCATCGC-3′, R = 5′-GGC CACAGCCCCTCTTGCCAG, LacZ = 5′-TGCGCAACTGTT GGGAAGGGCGATC-3′).

X-Gal staining

For the staining of whole embryos, embryos were fixed with 2% PFA and 0.2% glutaraldehyde in PBS for 30 min at 4°C, rinsed with PBS, and incubated for 3–4 h at 37 °C or overnight at room temperature in the staining solution containing 5-bromo-4-chloro-3-indolyl-β-D-galactopyranoside (X-Gal). For the staining of specimens, frozen sections were prepared as described above, post-fixed with 0.2% PFA/PBS, permeabilized by 0.01% sodium-deoxycolate, 0.02% NP-40 and 2 mM $MgCl_2$ in PBS, and incubated for 3–4 h at 37 °C in the staining solution.

Histological analysis

Embryos were isolated, fixed overnight with 10% neutralized formalin, dehydrated, embedded in paraffin, sectioned, and stained with hematoxylin and eosin (H&E).

Transmission electron microscopy (TEM)

E10.5 embryos, whose hearts were still beating, were prefixed with a mixture of 4% paraformaldehyde and 0.3% glutaraldehyde in a 0.1 M cacodylate buffer for 12 h. Hearts were dissected from embryos, postfixed with 2% glutaraldehyde in a 0.1 M cacodylate buffer for 24 h and with 3% osmium tetroxide for another 3 h, dehydrated through an ethanol series, and embedded in Epon812. The hearts were then sectioned at 0.5 μm thickness, stained with toluidine blue, and examined by a light microscope. After careful examination for location and orientation of the sample, 80–90 nm sections were prepared, doubly stained with uranylacetate and lead citrate, and observed under a JEOL 2000EX electron microscope at 80 kV.

Acknowledgements

We thank T. Noda (Cancer Institute, Tokyo, Japan) for providing us with *nls-LacZ* plasmid. This work was supported in part by a grant-in-aid from the Ministry of Health, Labor and Welfare of Japan for the 3rd-term Comprehensive 10-year Strategy for Cancer Control. R. A. was an awardee of Research Fellowships of the Japan Society for the Promotion of Science for Young Scientists during this study. This manuscript was edited by NIH Fellows Editorial Board.

References

Abdelwahid, E., Pelliniemi, L.J., Szucsik, J.C., Lessard, J.L. & Jokinen. E. (2004) Cellular disorganization and extensive apoptosis in the developing heart of mice that lack cardiac muscle α-actin: apparent cause of perinatal death. *Pediatr. Res.* **55**, 197–204.

Ajima, R., Kajiya, K., Inoue, T., Tani, M., Shiraishi-Yamaguchi, Y., Maeda, M., Segawa, T., Furuichi, T., Sutoh, K. & Yokota, J. (2007) HOMER2 binds MYO18B and enhances its activity to suppress anchorage independent growth. *Biochem. Biophys. Res. Commun.* **356**, 851–856.

Arber, S., Hunter, J.J., Ross, J. Jr., Hongo, M., Sansig, G., Borg, J., Perriard, J.C., Chien, K.R. & Caroni. P. (1997) MLP-deficient mice exhibit a disruption of cardiac cytoarchitectural organization, dilated cardiomyopathy, and heart failure. *Cell* **88**, 393–403.

Arimura, T., Hayashi, T., Terada, H. *et al.* (2004) A Cypher/ZASP mutation associated with dilated cardiomyopathy alters the binding affinity to protein kinase C. *J. Biol. Chem.* **279**, 6746–6752.

Berg, J.S., Powell, B.C. & Cheney, R.E. (2001) A millennial myosin census. *Mol. Biol. Cell.* **12**, 780–794.

Chien, K.R. (2000) Genomic circuits and the integrative biology of cardiac diseases. *Nature* **407**, 227–232.

© 2008 The Authors
Journal compilation © 2008 by the Molecular Biology Society of Japan/Blackwell Publishing Ltd.

Chu, X., Chen, J., Reedy, M.C., Vera, C., Sung, K.L. & Sung, L.A. (2003) E-Tmod capping of actin filaments at the slow-growing end is required to establish mouse embryonic circulation. *Am. J. Physiol. Heart Circ. Physiol.* **284**, H1827–H1838.

Edmondson, D.G., Edmondson, D.G., Lyons, G.E., Martin, J.F. & Olson, E.N. (1994) Mef2 gene expression marks the cardiac and skeletal muscle lineages during mouse embryogenesis. *Development* **120**, 1251–1263.

Ervasti, J.M. (2003) Costameres: the Achilles' Heel of Herculean Muscle. *J. Biol. Chem.* **278**, 13591–13594.

Frank, D., Kuhn, C., Katus, H.A. & Frey, N. (2006) The sarcomeric Z-disc: a nodal point in signalling and disease. *J. Mol. Med.* **84**, 446–468.

Honda, H., Oda, H., Nakamoto, T., Honda, Z., Sakai, R., Suzuki, T., Saito, T., Nakamura, K., Nakao, K., Ishikawa, T., Katsuki, M., Yazaki, Y. & Hirai, H. (1998) Cardiovascular anomaly, impaired actin bundling and resistance to Src-induced transformation in mice lacking p130Cas. *Nat. Genet.* **19**, 361–365.

Isogawa, Y., Kon, T., Inoue, T., Ohkura, R., Yamakawa, H., Ohara, O. & Sutoh, K. (2005) The N-terminal domain of MYO18A has an ATP-insensitive actin-binding site. *Biochemistry* **44**, 6190–6196.

Knoll, R., Hoshijima, M., Hoffman, H.M. *et al.* (2002) The cardiac mechanical stretch sensor machinery involves a Z disc complex that is defective in a subset of human dilated cardiomyopathy. *Cell* **111**, 943–955.

Liang, Y., Wang, A., Belyantseva, I.A. *et al.* (1999) Characterization of the human and mouse unconventional myosin XV genes responsible for hereditary deafness DFNB3 and shaker 2. *Genomics* **61**, 243–258.

Mermall, V., Post, P.L. & Mooseker, M.S. (1998) Unconventional myosins in cell movement, membrane traffic, and signal transduction. *Science* **279**, 527–533.

Milner, D.J., Weitzer, G., Tran, D., Bradley, A. & Capetanaki, Y. (1996) Disruption of muscle architecture and myocardial degeneration in mice lacking desmin. *J. Cell. Biol.* **134**, 1255–1270.

Mohapatra, B., Jimenez, S., Lin, J.H., Bowles, K.R., Coveler, K.J., Marx, J.G., Chrisco, M.A., Murphy, R.T., Lurie, P.R., Schwartz, R.J., Elliott, P.M., Vatta, M., McKenna, W., Towbin, J.A. & Bowles, N.E. (2003) Mutations in the muscle LIM protein and α-actinin-2 genes in dilated cardiomyopathy and endocardial fibroelastosis. *Mol. Genet. Metab.* **80**, 207–15.

Nakano, T., Tani, M. Nishioka, M., Kohno, T., Otsuka, A., Ohwada, S. & Yokota, J. (2005) Genetic and epigenetic alterations of the candidate tumor-suppressor gene MYO18B, on chromosome arm 22q, in colorectal cancer. *Genes Chromosomes Cancer* **43**, 162–171.

Nishioka, M., Kohno, T., Tani, M., Yanaihara, N., Tomizawa, Y., Otsuka, A., Sasaki, S., Kobayashi, K., Niki, T., Maeshima, A., Sekido, Y., Minna, J.D., Sone, S. & Yokota, J. (2002) MYO18B, a candidate tumor suppressor gene at chromosome 22q12.1, deleted, mutated, and methylated in human lung cancer. *Proc. Natl. Acad. Sci. USA* **99**, 12269–12274.

Salamon, M., Millino, C., Raffaello, A., Mongillo, M., Sandri, C., Bean, C., Negrisolo, E., Pallavicini, A., Valle, G., Zaccolo, M., Schiaffino, S. & Lanfranchi, G. (2003) Human MYO18B, a novel unconventional myosin heavy chain expressed in striated muscles moves into the myonuclei upon differentiation. *J. Mol. Biol.* **326**, 137–149.

Takeda, K., Kishi, H., Ma, X., Yu, Z.X. & Adelstein R.S. (2003) Ablation and mutation of nonmuscle myosin heavy chain II-B results in a defect in cardiac myocyte cytokinesis. *Circ. Res.* **93**, 330–337.

Takeda, K., Yu, Z.X., Qian, S., Chin, T.K., Adelstein, R.S. & Ferrans, V.J. (2000) Nonmuscle myosin II localizes to the Z-lines and intercalated discs of cardiac muscle and to the Z-lines of skeletal muscle. *Cell Motil. Cytoskeleton* **46**, 59–68.

Tani, M., Ito, J., Nishioka, M., Kohno, T., Tachibana, K., Shiraishi, M., Takenoshita, S. & Yokota, J. (2004) Correlation between histone acetylation and expression of the MYO18B gene in human lung cancer cells. *Genes Chromosomes Cancer* **40**, 146–151.

Tullio, A.N., Accili, D., Ferrans, V.J., Yu, Z.X., Takeda, K., Grinberg, A., Westphal, H., Preston, Y.A. & Adelstein, R.S. (1997) Nonmuscle myosin II-B is required for normal development of the mouse heart. *Proc. Natl. Acad. Sci. USA* **94**, 12407–12412.

Uren, D., Hwang, H.K., Hara, Y., Takeda, K., Kawamoto, S., Tullio, A.N., Yu, Z.X., Ferrans, V.J., Tresser, N., Grinberg, A., Preston, Y.A. & Adelstein R.S. (2000) Gene dosage affects the cardiac and brain phenotype in nonmuscle myosin II-B-depleted mice. *J. Clin. Invest.* **105**, 663–671.

Wu, X., Jung, G. & Hammer, J.A. 3rd. (2000) Functions of unconventional myosins. *Curr. Opin. Cell Biol.* **12**, 42–51.

Yanaihara, N., Nishioka, M., Kohno, T., Otsuka, A., Okamoto, A., Ochiai, K., Tanaka, T. & Yokota, J. (2004) Reduced expression of MYO18B, a candidate tumor-suppressor gene on chromosome arm 22q, in ovarian cancer. *Int. J. Cancer* **112**, 150–154.

Zhou, Q., Chu, P.H., Huang, C., Cheng, C.F., Martone, M.E., Knoll, G., Shelton, G.D., Evans, S. & Chen, J. (2001) Ablation of Cypher, a PDZ-LIM domain Z-line protein, causes a severe form of congenital myopathy. *J. Cell Biol.* **155**, 605–612.

Received: 15 March 2008
Accepted: 30 June 2008

© 2008 The Authors
Journal compilation © 2008 by the Molecular Biology Society of Japan/Blackwell Publishing Ltd.

ELSEVIER

International Journal of Cardiology 125 (2008) 286–287

International Journal of Cardiology

www.elsevier.com/locate/ijcard

Letter to the Editor

Takayasu arteritis evaluated by multi-slice computed tomography in an old man

Tetsuo Fujita [a], Masashi Ohtsuka [a,*], Eiji Uchida [a], Hiroyuki Yamaguchi [a], Toru Nakajima [a], Hiroshi Akazawa [b], Hiroyuki Takano [b], Haruaki Nakaya [c], Issei Komuro [b]

[a] *Department of Cardiology, Seirei Yokohama General Hospital, 215 Iwai-cho, Hodogaya-ku, Yokohama 240-8521, Japan*
[b] *Cardiovascular Science and Medicine, Chiba University Graduate School of Medicine, 1-8-1 Inohana, Chuo-ku, Chiba 260-8670, Japan*
[c] *Department of Pharmacology, Chiba University Graduate School of Medicine, 1-8-1 Inohana, Chuo-ku, Chiba 260-8670, Japan*

Received 16 March 2007; accepted 26 May 2007
Available online 24 August 2007

Abstract

In the case of patients with Takayasu arteritis (TA), they consult a doctor for the first time when they have a slight fever, shoulder pain, chest pain, back pain, or headache, or when they are pointed out to have high CRP or anemia by chance in medical check-up. In TA, they are usually young women. In our case, the very old patient had bilateral massive pleural effusion and aortic aneurysm with a 64-slice computed tomography (CT). TA commonly affects primarily large elastic arteries such as the aorta and its main branches. Steroid was very effective for suppression of inflammatory symptom being dose-dependent. His pleural effusion had been decreasing without reducing the size of aortic aneurysm. Multi-slice CT was a very useful tool to detect unexpected lesion in Takayasu arteritis in a non-invasive manner.
© 2007 Elsevier Ireland Ltd. All rights reserved.

Keywords: Takayasu arteritis; Multi-slice CT; Matrix metalloproteinases

1. Case report

In August 2007, a 94-year-old man was admitted to the hospital with low appetite, left shoulder pain and slight fever rising. He had hypertension, but his eye ground findings were not particular. He didn't show extremities claudication, bruit, blood pressure asymmetries and pulse asymmetries. White blood cell counts, liver and renal function were normal. He had inflammatory anemia (Hb 8.8 g/dl, UIBC 81 μg/dl, TIBC 95 μg/dl) and high C-reactive protein (CRP) (9.4 mg/dl). His antinuclear antibody was positive (320 times) and his complement activity was low in blood serum. On the other hand, bacterial culture and other evidence for secondary vasculitis due to other inflammatory indicators (p-ANCA, c-ANCA) were negative. Ultrasonic echocardiography showed only mild left ventricular hypertrophy due to hypertension. It did not show aortic regurgitation and normal left ventricular wall motion. A 64-slice computed tomography (CT) showed bilateral massive pleural effusion and aortic aneurysm with mural thrombus (arrow in Fig. 1A) and wall thickening in aortic arch (arrowhead in Fig. 1B). But we had detected no stenosis on the three branches of aortic arch and no abdominal aortic aneurysm. We had thought that he had inflammatory aortic aneurysm (vasculitis syndrome) and we made a diagnosis of a part of aortic arch syndrome (Takayasu arteritis: TA) with diagnostic criteria by the Ministry of Health and Welfare in Japan. We administrated predonisolone (PSL) 20 mg/day which decreased the fever and CRP decreased from 14.1 to 1.1 for 20 days. His pleural effusion had been decreasing without reducing the size of aortic aneurysm and we controlled PSL 20 mg. Steroid was very effective for suppression of inflammatory symptom being dose-dependent.

2. Discussion

In case of patients with aortic arch syndrome, they consult a doctor for the first time when they have a slight fever,

* Corresponding author. Tel.: +81 45 715 3111; fax: +81 45 715 3387.
E-mail address: masaootsuka-circ@umin.ac.jp (M. Ohtsuka).

0167-5273/$ - see front matter © 2007 Elsevier Ireland Ltd. All rights reserved.
doi:10.1016/j.ijcard.2007.05.041

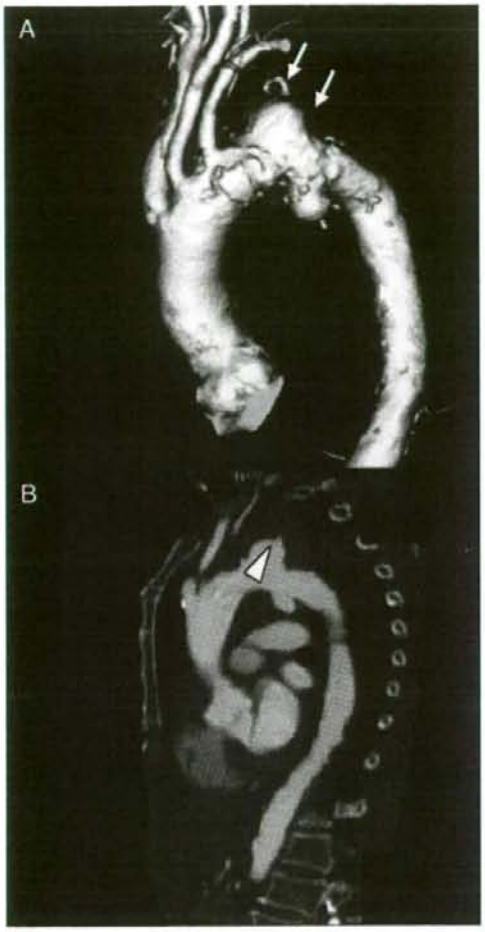

Fig. 1. (A) A 64-slice computed tomography (CT) showed massive aortic aneurysm (arrows), and (B) wall thickening in aortic arch (arrowhead).

shoulder pain, chest pain, back pain, or headache, or when they are pointed out to have high CRP or anemia by chance in medical check-up. In TA, women aged 20–30 years old are usually affected [1], and an old man in this case is very unique.

TA commonly affects primarily large elastic arteries such as the aorta and its main branches. We differentiated it from typical atherosclerosis, a disease much more likely to affect the lower extremity large vessels than the arms and the abdominal aorta than the aortic arch and root. Aneurysms are the most common and clinically most significant in the aortic root, where they can lead to valvular regurgitation. The earliest histological change appears to be a granulomatous inflammation in the adventia and outer layers of the affected arteries, followed by gradual progression to a panarteritis with inflammatory mononuclear cell infiltration. Inflammation and subsequent neointimal proliferation (intimal thickening) result in stenotic or occlusive lesions, whereas destruction of the elastica and muscularis may form dilatation or aneurysms [2]. In this process, proteases secreted from infiltrated cells are thought to play some role in the destruction of elastic fibers. Recently there was a report that matrix metalloproteinases (MMPs) are involved with inflammatory processes [3].

If they don't have appropriate therapy by steroid and inflammatory symptom is not well controlled, ischemic symptom, hypertension, and cardiac failure appear with progression of the disease. Multi-slice CT was a very useful tool to detect unexpected lesion in Takayasu arteritis in a non-invasive manner [4,5].

Because our patient was an old man, we did not expect that he had Takayasu arteritis. Since CT angiography was very helpful in detecting the aortic arch syndrome, we should further use multi-slice CT.

References

[1] Numano F, Okawara M, Inomata H, Kobanayashi Y. Takayasu's arteritis. Lancet 2000;356:1023–5.
[2] Kerr GS, Hallahan CW, Giordano J, et al. Takayasu arteritis. Ann Intern Med 1994;120:919–29.
[3] Matsuyama A, Sakai N, Ishigami M, et al. Matrix metalloproteinases as novel markers in Takayasu arteritis. Circulation 2003;108:1469–73.
[4] Ando H, Funabashi N, Uehara M, et al. Abnormal collateral arterial systems in Takayasu's arteritis and Lerieche's syndrome evaluated by whole body acquisition using multislice computed tomography. Int J Cardiol 2007;121:306–8.
[5] Ohtsuka M, Uchida E, Yamaguchi H, et al. Coronary aneurysm reduced after coronary stenting. Int J Cardiol 2007;121:76–7.

ELSEVIER

International Journal of Cardiology 128 (2008) 294–295

International Journal of Cardiology

www.elsevier.com/locate/ijcard

Letter to the Editor

Abdominal aortic pseudoaneurysm caused by prolonged methicillin-resistant *Staphylococcus aureus* sepsis

Takanobu Utsumi [a], Masashi Ohtsuka [a,*], Eiji Uchida [a], Hiroyuki Yamaguchi [a], Toru Nakajima [a], Hiroshi Akazawa [b], Hiroyuki Takano [b], Haruaki Nakaya [c], Issei Komuro [b]

[a] *Department of Cardiology, Seirei Yokohama General Hospital, 215 Iwai-cho, Hodogaya-ku, Yokohama 240-8521, Japan*
[b] *Department of Cardiovascular Science and Medicine, Chiba University Graduate School of Medicine, 1-8-1 Inohana, Chuo-ku, Chiba 260-8670, Japan*
[c] *Department of Pharmacology, Chiba University Graduate School of Medicine, 1-8-1 Inohana, Chuo-ku, Chiba 260-8670, Japan*

Received 21 March 2007; accepted 15 June 2007
Available online 24 October 2007

Abstract

The mechanism of pseudoaneurysm formation caused by prolonged sepsis is thought to be related to the vascular endothelium being directly invaded and broken by bacteria. Moreover, matrix metalloproteinases (MMPs) which are up-regulated by chronic inflammation have been reported to be implicated in the pathogenesis of aneurysm development through increased proteolysis of extracellular matrix proteins. An effective treatment for infected pseudoaneurysm remains unsettled. Surgery is generally performed, however, because the patients in most of these cases are in very poor physical condition, the operation is associated with high morbidity and mortality. A more successful alternative is endovascular treatment. Recent reports indicate low morbidity and mortality rates with this treatment. If the patient in this case had been in better condition, we could have selected endovascular stent-grafting for her treatment.
© 2007 Elsevier Ireland Ltd. All rights reserved.

Keywords: Pseudoaneurysm; Multi-slice CT; Matrix metalloproteinases

1. Case report

In October 2006, a 77-year-old woman underwent pancreatoduodenectomy for a malignant pancreatic tumor. On the 8th postoperative day, her temperature was 39.3 °C. At that time, laboratory tests showed a white cell count of $1.82 \times 10^4/\mu l$ and a C-reactive protein (CRP) of 5.6 mg/dl. The central venous catheter tip and blood cultures were positive for methicillin-resistant *Staphylococcus aureus* (MRSA). In view of antibiotic sensitivity test results, arbekacin (ABK) was the most sensitive to MRSA and the treatment with ABK was started. On the 13th postoperative day, she suddenly complained of right inguinal pain and lumbar pain. Abdominal and pelvic X-ray revealed no abnormal findings. A 64-slice computed tomography (CT) resulted in the same (Fig. 1A and B). However, the patient continued to complain of the lumbar pain. A second series of blood cultures made after 15 days of the treatment with ABK were still positive for MRSA. Therefore, ABK treatment was changed into vancomycin (VCM). On the 31st postoperative day, the 64-slice CT for the second time showed that a 2.1-cm false aneurysm of abdominal aortaproximal to the divergence of common iliac artery (Fig. 1C and D). We consulted cardiac surgeons about indication of the surgery, however, surgery was ruled out owing to her greatly weaken condition. Although medication was continued, patient's hypotension and MRSA sepsis were not controlled. On the 72nd postoperative day, she died of progressive renal failure.

2. Discussion

Pseudoaneurysm is usually known to be caused by trauma [1] and surgical treatment [2] but rarely MRSA infection.

* Corresponding author. Tel.: +81 45 715 3111; fax: +81 45 715 3387.
E-mail address: masaootsuka-circ@umin.ac.jp (M. Ohtsuka).

0167-5273/$ - see front matter © 2007 Elsevier Ireland Ltd. All rights reserved.
doi:10.1016/j.ijcard.2007.06.043

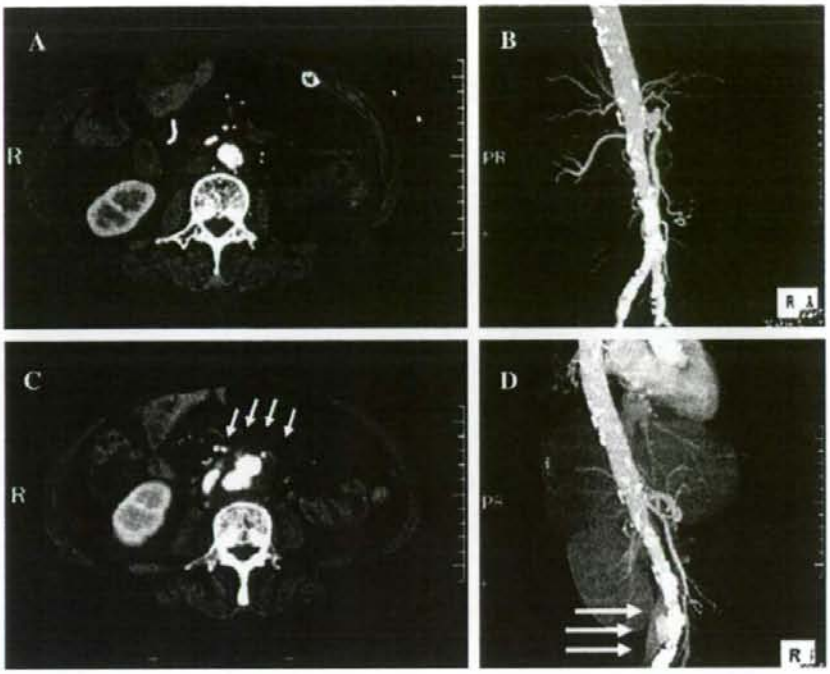

Fig. 1. Multi-slice CT changes shown in abdominal aortic pseudoaneurysm. A 64-slice CT revealed no abnormal findings (A, B). On the 31st postoperative day, the 64-slice CT for the second time showed that a 2.1-cm false aneurysm of abdominal aorta proximal to the divergence of common iliac artery (arrows) (C, D).

This case was thought to have been caused by prolonged MRSA sepsis based on the comparison between CT findings for the first time (Fig. 1A and B) with for second time (Fig. 1C and D). Additionally, it was hardly possible that abdominal aorta had been injured by the surgical procedure in view of its site.

If we suspect pseudoaneurysm with infection, multi-slice CT may be a useful tool in detecting unexpected lesion in a non-invasive manner [3,4]. In fact, CT angiography was very helpful in detecting the pseudoaneurysm and we should further use multi-slice CT.

The mechanism of pseudoaneurysm formation caused by prolonged sepsis is thought to be related to the vascular endothelium being directly invaded and broken by bacteria. Moreover, matrix metalloproteinases (MMPs) which are up-regulated by chronic inflammation have been reported to be implicated in the pathogenesis of aneurysm development through increased proteolysis of extracellular matrix proteins [5].

An effective treatment for infected pseudoaneurysm remains unsettled. Surgery is generally performed, however, because the patients in most of these cases are in very poor physical condition, the operation is associated with high morbidity and mortality [6]. A more successful alternative is endovascular treatment. Recent reports indicate low morbidity and mortality rates with this treatment [6]. If the patient in this case had been in better condition, we could have selected endovascular stent-grafting for her treatment.

References

[1] Chai P, Mohiaddin R. Traumatic pseudoaneurysm of the descending thoracic aorta. Circulation 2005;112:e260–1.
[2] Heise M, Werk M, Husmann I, et al. Rapid development of multiple pseudoaneurysms after arterial homograft placement. Circulation 2006;114:e80–1.
[3] Chambers ST. Diagnosis and management of staphylococcal infections of vascular grafts and stents. Intern Med J 2005;35:s72–8.
[4] Ohtsuka M, Uchida E, Yamaguchi H, et al. Coronary aneurysm reduced after coronary stenting. Int J Cardiol 2007;121:76–7.
[5] Yoshimura K, Aoki H, Ikeda Y, et al. Regression of abdominal aortic aneurysm by inhibition of c-Jun N-terminal kinase. Nat Med 2005;11:1330–8.
[6] Sanada J, Matsui O, Arakawa F, et al. Endovascular stent-grafting for infected iliac artery peudoaneurysms. Cardiovasc Interv Radiol 2005;28:83–6.

www.nature.com/clinicalpractice/cardio

Vascular aging: insights from studies on cellular senescence, stem cell aging, and progeroid syndromes

Tohru Minamino and Issei Komuro*

SUMMARY

Epidemiological studies have shown that age is the chief risk factor for atherosclerotic cardiovascular diseases, but the molecular mechanisms that underlie the increase in risk conferred by aging remain unclear. Evidence suggests that the cardiovascular repair system is impaired with advancing age, thereby inducing age-associated cardiovascular dysfunction. Such impairment could be attributable to senescence of cardiovascular tissues at the cellular level as a result of telomere shortening, DNA damage, and genomic instability. In fact, the replicative ability of cardiovascular cells, particularly stem cells and/or progenitor cells, has been shown to decline with age. Recently, considerable progress has been made in understanding the pathogenesis of human progeroid syndromes that feature cardiovascular aging. Most of the genes responsible have a role in DNA metabolism, and mutated forms of these genes result in alterations of the response to DNA damage and in decreased cell proliferation, which might be common features of a phenotype of aging. Here we review the cardiovascular research on cellular senescence, stem cell aging, and progeroid syndromes and discuss the potential role of cellular senescence in the mechanisms underlying both normal aging and premature aging syndromes.

KEYWORDS DNA damage, progenitor cell, progeria, senescence, telomere

REVIEW CRITERIA

We searched PubMed for papers published between 1980 and 2008 by using combinations of the following search terms: "aging", "senescence", "telomere", "stem cell", "progenitor cell", "EPC", "progeroid", "Hutchinson–Gilford progeria syndrome" and "Werner syndrome". We also searched the reference lists of papers identified for other relevant manuscripts.

T Minamino is Assistant Professor at the Department of Cardiovascular Science and Medicine, Chiba University Graduate School of Medicine, and a Research Scientist at Japan Science and Technology Agency, Saitama, and I Komuro is Professor and Chairman of the Department of Cardiovascular Science and Medicine at Chiba University Graduate School of Medicine and Director of the Center for Cardiovascular Interventions at Chiba University Hospital, Chiba, Japan.

Correspondence
*Department of Cardiovascular Science and Medicine, Chiba University Graduate School of Medicine, 1-8-1 Inohana, Chuo-ku, Chiba 260-8670, Japan
komuro-tky@umin.ac.jp

Received 4 March 2008 **Accepted** 1 July 2008 **Published online** 2 September 2008
www.nature.com/clinicalpractice
doi:10.1038/ncpcardio1324

INTRODUCTION

Aging is a known major risk factor for cardiovascular disease.[1] The aging process is also associated with adverse hemodynamic and metabolic changes that accelerate the development of cardiovascular disease. It is now accepted that changes in cardiovascular structure and function occur in healthy individuals as they age. These alterations precede the onset of clinical disease and predict the future risk of developing atherosclerosis, hypertension and heart failure. Such age-related changes could, therefore, be potential targets for new treatments.

The age-associated changes in blood vessels that occur in healthy individuals include increased arterial wall thickness, luminal dilatation and reduced compliance.[2] In addition to these structural changes, endothelial function becomes impaired with increasing age, thereby increasing arterial stiffness.[2] This endothelial dysfunction is partly caused by decreased production of vasodilators, such as nitric oxide and prostacyclin, and a reduction in the responsiveness of vascular smooth muscle cells (VSMCs) to these vasodilators. Moreover, evidence indicates that cardiovascular repair systems become progressively impaired with aging. For example, neovascularization of ischemic tissue and re-endothelialization after vascular injury are impaired in aged animals.[3,4] These impairments are attributed to the reduced production of proangiogenic factors, impaired cell replication, and a decrease in the number and function of stem and/or progenitor cells. Even if these age-associated changes do not result in overt cardiovascular disease *per se*, they impair the capacity of the cardiovascular system and influence the severity and prognosis of subsequent disease.

Cellular and molecular mechanisms underlying age-associated changes of the cardiovascular system have been studied, but it remains unclear exactly how these alterations occur with advancing age. Evidence suggests that cardiovascular cells, including stem and/or progenitor cells, undergo senescence, and that this process

© 2008 Macmillan Publishers Limited. All rights reserved